RADIO SCIENCE, VOL. 48, 416–426, doi:10.1002/rds.20047, 2013

Development of a passive VHF radar system using software-defined radio for equatorial plasma instability studies

B. Tuysuz,[1] J. Urbina,[1] and F. D. Lind[2]

Received 31 July 2012; revised 10 June 2013; accepted 15 June 2013; published 9 August 2013.

[1] In this paper, a bistatic passive radar receiver system named "Coherent-scatter Atmospheric Passive Radar Imager (CAPRI)" is described. It is primarily designed to study the dynamics of the upper atmosphere by utilizing "transmitters of opportunity" as the RF target illuminators. CAPRI is constructed using the open source software-defined radio toolkit, GNU Radio, to meet the signal processing requirements in combination with the open source hardware, Universal Software Radio Peripheral 2, for data acquisition. The resultant system is highly flexible, and we present the details of the design as well as a performance analysis. CAPRI will be deployed in Peru, near the magnetic equator, for long-term operations in the area. FM stations near Lima, Peru, will be utilized with the targets of interest being the equatorial electrojet and the spread F. The results will then be compared to the Jicamarca Unattended Long-term investigations of the Ionosphere and Atmosphere (JULIA) radar data, and CAPRI will be used to improve the simultaneous time and spatial coverage in the region in a more cost-effective manner.

Citation: Tuysuz, B., J. Urbina, and F. D. Lind (2013), Development of a passive VHF radar system using software-defined radio for equatorial plasma instability studies, *Radio Sci.*, *48*, 416–426, doi:10.1002/rds.20047.

1. Introduction

[2] Ionospheric *F* region irregularities and its corresponding electrodynamic precursors are one of the oldest topics in equatorial aeronomy [*Woodman*, 2009]. Today, we still struggle to provide simultaneous time and spatial coverage on key ionospheric parameters, such as vertical and zonal plasma drifts and their daytime variabilities. Furthermore, the Earth's distribution of ionization is significantly affected by the equatorial electric fields and plasma drifts through the "fountain effect" [*Martyn*, 1955]. Development of realistic ionospheric models of this phenomena would greatly benefit from continuous and cost-effective observations of the lower ionosphere [*Fejer et al.*, 1995].

[3] Coherent scatter radar provides convenient and capable means to probe the low-latitude ionosphere. The detection of coherent scatter echoes from *E* and *F* region **B**-field aligned irregularities (FAI) requires a radar **k**-vector to be oriented perpendicular to the **B** field. This approach can be easily implemented at equatorial latitudes, near the geomagnetic equator. Even though Jicamarca Radio Observatory (JRO) can observe ionospheric irregularities and neutral atmosphere for extended periods of time in Jicamarca Unattended Long-term investigations of the Ionosphere and Atmosphere (JULIA) mode, this radar configuration does not, in general, provide continuous data due to the operational constraints and the need to perform other interfering experiments [*Hysell and Burcham*, 2002].

[4] As an alternative to the traditional radar sensing systems and techniques, the detection of FAI scattering from commercial FM transmitters can be utilized using a passive radar receiver system. This approach to monitoring the ionosphere can be operated continuously and used to provide wide spatial coverage of the unstable ionosphere [*Sahr and Meyer*, 2004]. Also, utilization of the third party transmitters reduce the cost of instrumentation and provides diversity in frequency and scattering geometry.

[5] There has been extensive investigation of passive radar systems as a means for tracking nongeophysical targets such as aircraft [e.g., *Griffiths and Long*, 1986]. These studies involved various kinds of "transmitters of opportunity" such as satellite, analog television, and FM radio signals. However, the waveform used should satisfy two requirements for radar applications. It needs to provide a useful self-ambiguity response, and the illumination must be sufficiently powerful. GPS satellite waveforms are superb for range and Doppler estimation. Unfortunately, they are inadequate for passive radar implementation since they are too weak to provide adequate illumination for nearly anything except forward scatter. On the other hand, analog television waveforms are powerful and provide good illumination, but the ambiguity in the signal greatly reduces the successful detection rate of the tracking

[1]Department of Electrical Engineering, Pennsylvania State University, University Park, Pennsylvania, USA.
[2]MIT Haystack Observatory, Massachusetts Institute of Technology, Westford, Massachusetts, USA.

Corresponding author: B. Tuysuz, Department of Electrical Engineering, Pennsylvania State University, 218 Electrical Engineering East, University Park, Pennsylvania 16802, USA. (buraktuysuz@gmail.com)

0048-6604/13/10.1002/rds.20047

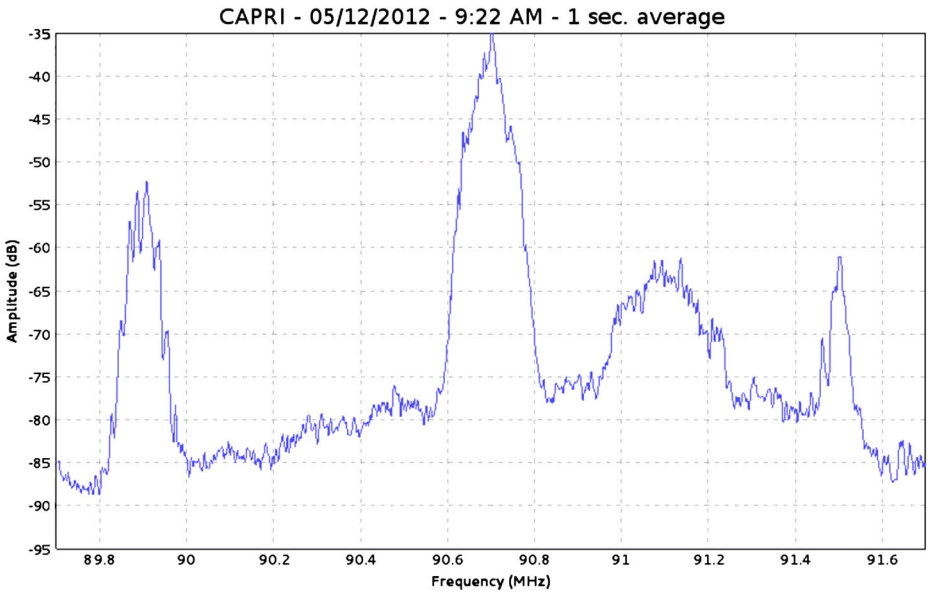

Figure 1. Time-averaged FM power spectrum of a 2 MHz signal at 90.7 MHz, State College, PA, USA.

systems. A comprehensive performance analysis of commercial broadcasts used for passive radar operation and several earlier operational examples are given in *Griffiths and Baker* [2005] and *Baker et al.* [2005]. A more recent passive radar system, developed for ionospheric research, is the Manastash Ridge Radar (MRR) [*Sahr and Lind*, 1997]. This system was built to study electrodynamic turbulence in the ionosphere, specifically auroral *E* region FAI, using range and Doppler measurements derived from FM broadcast transmitters.

[6] In contrast to the previously cited successful passive radar studies, observations using FM radio frequency bands have never been conducted at the magnetic equator near Peru. Such observations are expected to provide complementary data information to the geophysical sensors available at JRO. The development of low-cost digital receivers, software-defined radio techniques, and GPS-derived synchronization has enabled the development of compact and inexpensive passive radar systems. These systems are very flexible and enable easy exploitation of multiple "transmitters of opportunity" for passive radar observations. The deployment of CAPRI in Peru will be for future ionospheric studies.

[7] In section 2, an overview of the FM broadcasts is given. A performance evaluation of the FM waveform is provided in section 3, by using the data from CAPRI. In section 4, details of both the hardware and the software are discussed, and specifications of the system and operation are given. Potential CAPRI receiver locations in Peru are evaluated in section 5. Concluding remarks along with future work are given in section 6.

2. An Overview of FM Broadcasts

[8] In most parts of the world, commercial FM radios operate in the 88–108 MHz VHF band. These broadcast systems utilize a message signal $m(t)$ that modulates a carrier frequency f_c. A carrier waveform can be represented as follows,

$$s(t) = A\cos\left[2\pi f_c t + 2\pi k_f \int_{-\infty}^{t} m(\tau)\,\mathrm{d}\tau\right] \tag{1}$$

where A is a constant and k_f is the frequency sensitivity or the frequency deviation constant of the modulator. From equation (1), it is clear that, under ideal conditions, while the envelope is constant, the signal, $s(t)$, is a nonlinear function of the message signal, $m(t)$.

[9] Typical characteristics of FM broadcasts such as carrier separation, bandwidth, and transmitter power levels depend on local regulations. An example power spectrum, which shows four FM broadcasts in State College is given in Figure 1. Contrary to the regulations, the power spectrum indicates different effective bandwidths from 100 to 300 kHz in the same region. In a flexible passive radar receiver, which can be tuned to any FM channel, bandwidth adjustment and filtering without any hardware modification is essential to reduce the received noise level and to maximize the achievable instantaneous dynamic range.

3. Detection Performance Analysis of FM Broadcast

[10] The capability of detecting multiple targets with respect to their spatial and speed differences are key design goals for a radar system. These parameters depend highly on the quality of the radar signal. Hence, a resolution analysis is essential prior to use the signal for ionospheric research. The most convenient way to assess the target resolution of a signal is by analyzing its self-ambiguity function, which is a two-dimensional array in time delay and Doppler frequency

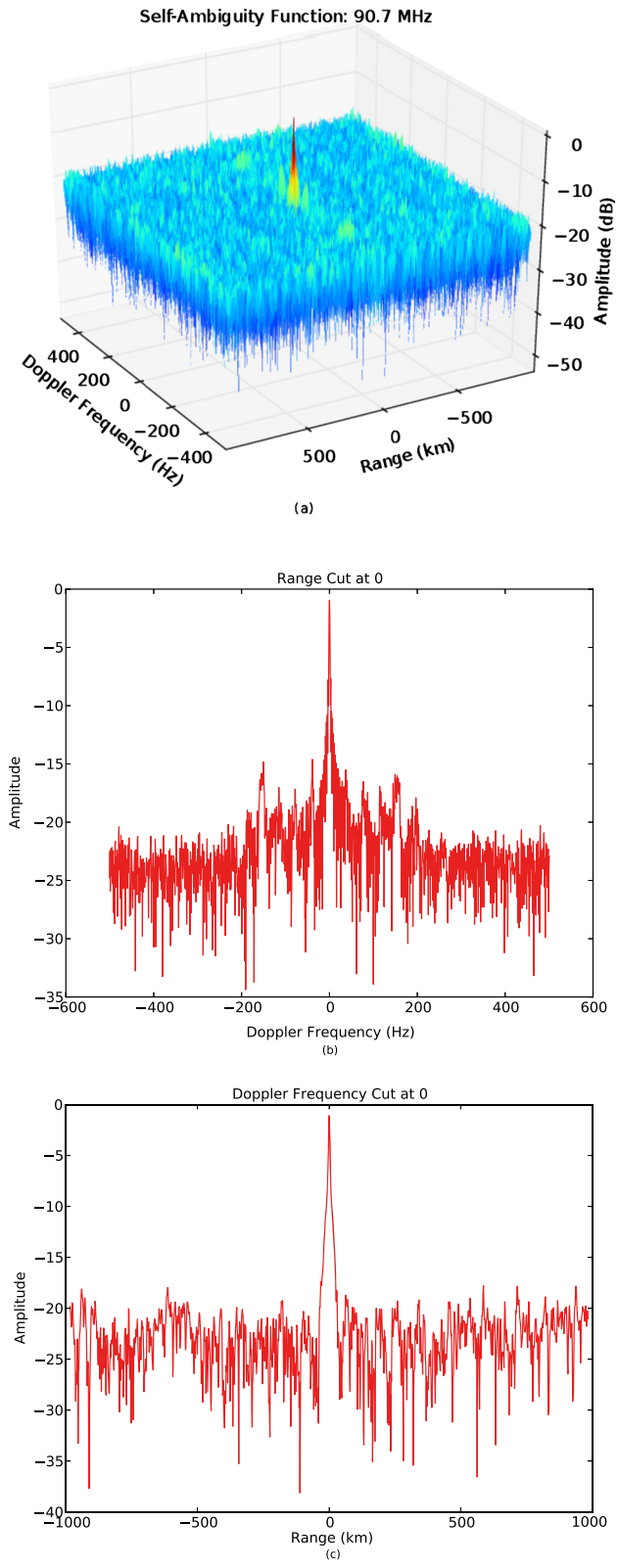

Figure 2. Self-ambiguity function plot of a music broadcast which is captured at 90.7 MHz by CAPRI receiver in State College, Pennsylvania. (200 kHz sampling rate for 0.5 s) (a) Three-dimensional plot of the ambiguity function. (b) Range cut at 0 km. (c) Doppler frequency cut at 0 Hz.

that represents the output of the matched filter [*Siebert*, 1956; *Levanon*, 1988]. It is given by:

$$|A(\tau,\upsilon)|^2 = \left| \int_{-\infty}^{\infty} s(t)s^*(t-\tau)e^{-j2\pi\upsilon t}\mathrm{d}t \right|^2 \qquad (2)$$

where $A(\tau,\upsilon)$ is the self-ambiguity response at time delay τ and Doppler frequency υ. Computation of this function tests the matched filter response of the signal $s(t)$ at different Doppler frequencies and time delays, thus producing a peak where the perfect matching occurs at $\tau = 0$ and $\upsilon = 0$ [*Stein*, 1981]. Extension of the peak in time delay and Doppler frequency axis indicates the time (or range) and the Doppler frequency resolutions of the signal, $s(t)$. Likewise, sidelobes in the self-ambiguity function of $s(t)$ may lead to the multiple detection of a single target.

[11] In conventional radar systems, substituting the radar waveform with $s(t)$ in equation (2), gives the resolution performance. On the other hand, in passive radar systems, where the radar signal is not known, a captured signal from the transmitter can be used in order to compute the self-ambiguity function. As an example, in Figure 2, the self-ambiguity function of the FM broadcast at 90.7 MHz is given. This particular plot shows 10 km range and 15 Hz Doppler frequency resolution corresponding to 0.5 s of data gated at 200 kHz sampling rate. Doppler frequency resolution can be further increased with longer integration times, and the range resolution depends on the bandwidth of the FM broadcast used.

[12] The self-ambiguity function behavior changes according to the instantaneous modulation of the FM signal, thus changing the Doppler frequency and the range resolution. This effect can be clearly noticed when the spectral content of the transmitted signal rapidly changes in time. Modulated rapid tempo music provides the best time and Doppler frequency resolution. By contrast, signal with speech content noticeably reduces the quality of the self-ambiguity response as shown in Figure 3. This test data was captured during a news announcement. Natural pauses occurring in human speech, which introduces gaps in the audio signal, are the primary cause of this reduced performance [*Baker et al.*, 2005].

[13] In passive radar systems, wide variations in utilized FM broadcast radio program content result in a random performance degradation of the range/Doppler detection capability. CAPRI utilizes multiple transmitters to help address the variation in transmit signal quality. This approach, which is discussed in section 4, also provides wavelength and **k**-vector diversity on the observations.

4. Description of the CAPRI

[14] A typical VHF passive radar system utilizes two receivers in a bistatic manner. A receiver is installed relatively close in range to the appropriate FM radio transmitters to obtain a reference copy of the transmitted signal. A second receiver is placed to detect the signal scattered by the FAI, with isolation provided by physical distance, obstacles, or spatial filtering from an appropriate antenna pattern. Configuration in this manner reduces the relative strength of the direct signal and allows detection of the desired echoes from FAI with positive signal to clutter ratios (SCR). A graphical depiction of this geometry is shown in Figure 4.

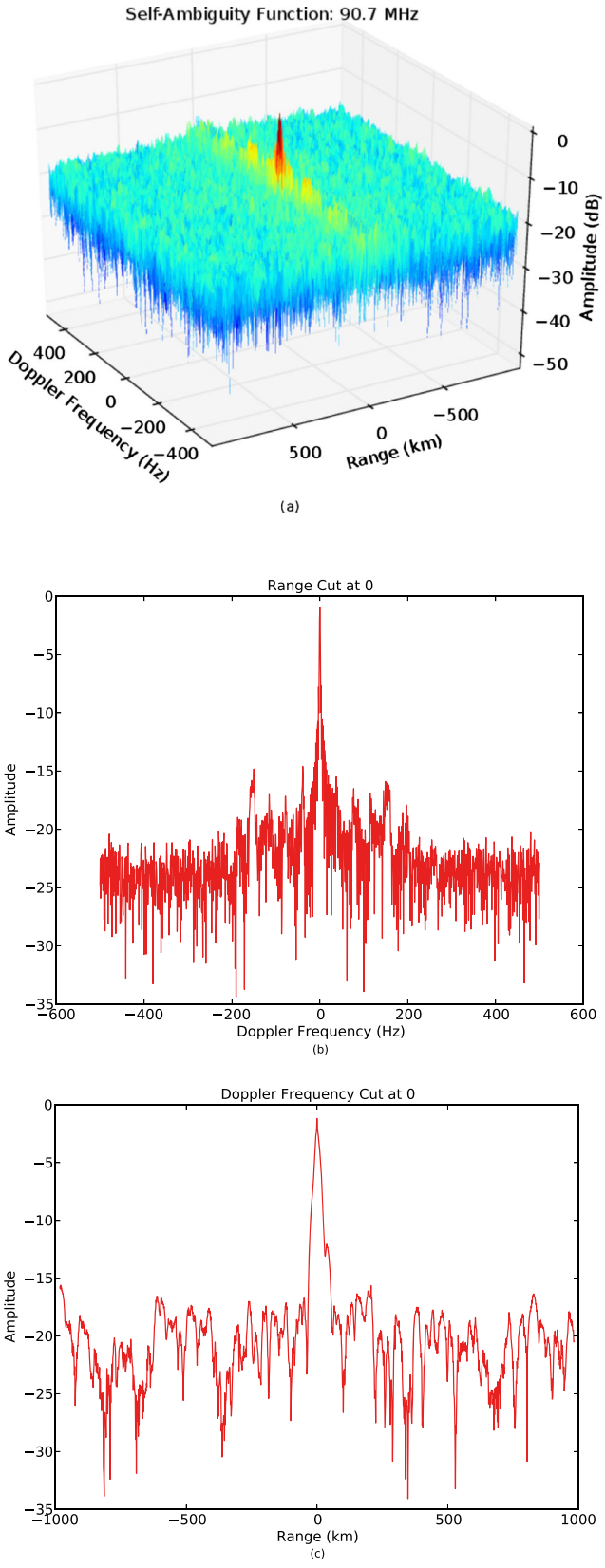

Figure 3. Self-ambiguity function plot of an announcement which is captured at 90.7 MHz by CAPRI receiver in State College (200 kHz sampling rate for 0.5 s). (a) Three dimensional plot of the ambiguity function. (b) Range cut at 0 km. (c) Doppler frequency cut at 0 Hz.

In many cases, multiple high power FM transmitters are colocated at a common site due to the logistics and maintenance costs which satisfy the opportunity of using multiple FM channels with the same passive radar setup. A flexible software-defined radio (SDR) supported multichannel radar receiver can take the advantage of this situation and operate at different frequencies simultaneously.

[15] The idea behind SDR is to have all real-time signal processing done with software instead of dedicated circuitry (e.g., filters, modulators, demodulators, and synchronizers) [*Dillinger et al.*, 2003]. In a passive radar, there are two main advantages of utilizing SDR in the system: first, receiver can be redesigned without modifying hardware. Second, the analog stages in a passive radar operation can be minimized. The GNU Radio (http://www.gnuradio.org) is an excellent open source SDR toolkit for these purposes. The SDR architecture is composed of individual signal processing blocks that are built using C++. Connections between these blocks are achieved using Python (http://www.python.org). There are about 100 signal processing blocks available in the toolkit, and it is also possible to add custom-designed signal processing blocks as necessary to implement a radio receiver (http://gnuradio.org/redmine/projects/gnuradio/wiki/Tutorials). Additionally, the Universal Software Radio Peripheral (USRP) (http://www.ettus.com) is a family of hardware platforms used for data acquisition which are compatible with GNU Radio.

[16] CAPRI utilizes the readily available open source GNU Radio SDR toolkit and the second generation USRP2 hardware to implement a very flexible VHF passive radar system. The hardware and software parts of the CAPRI are described in the following sections. Additional information about the CAPRI system can be found in *Tuysuz* [2012].

4.1. Hardware

[17] CAPRI consist of four main sections: an RF front-end, a digitizer hardware (USRP2), a global positioning system (GPS), and a computer to control the system. A block diagram of these sections and their interconnections are given in Figure 5. In this figure, the signal received from a log-periodic VHF antenna is passed through a low-noise amplifier that boosts the signal level. The next stage is an FM frequency band (88–108 MHz) antialiasing filter that suppresses out of band signals. The output of this filter is passed through a power splitter that provides the signals for two 14-bit analog to digital computers (ADCs), where the FM signal is sampled at F_s = 100 MHz. Since this sampling value is less than twice the Nyquist sampling frequency for a typical FM band, frequencies are aliased (f_{aliased}) and translated to an intermediate frequency (IF) by using equation (3), where n is an integer and f is the frequency of the IF:

$$f_{\text{aliased}} = |F_s * n - f| \tag{3}$$

[18] Since the typical bandwidth of an FM signal is around 200 kHz, the high speed sampling data rate can be reduced to mitigate data transfer and storage issues. Without loss of information, the sampling frequency F_s is reduced using complex baseband demodulation technique known as IQ-demodulation. This process consists of two main steps: down conversion and low-pass filtering with decimation. The down conversion stage is implemented

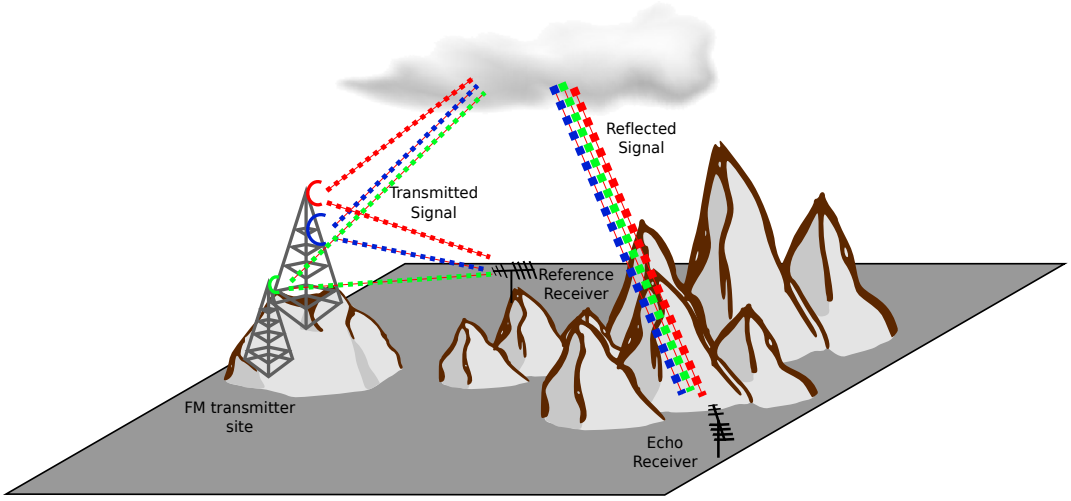

Figure 4. A typical passive radar geometry demonstration.

by multiplying the sampled, real-valued RF signal with a numerically controlled oscillator (NCO) reference signal. This operation produces a complex baseband signal at a rate of F_s = 100 MHz. This sampling rate is reduced using cascaded integrator-comb (CIC) filters which performs low-pass filtering and decimation at high speed [*Hogenauer*, 1981]. The variable decimation value provides the ability to adjust the bandwidth for the desired FM broadcast reception. After decimation of the baseband signal, 16-bit In-phase and 16-bit Quadrature samples are transferred to the host computer through an Ethernet port for each complex channel and stored in binary format for postprocessing.

[19] In a bistatic passive radar system, receivers may be widely separated. Therefore, time synchronization of each receiver is vital for data processing and interpretation. Proper range alignment of samples benefits greatly from highly accurate timing in the 100 ns or better range, especially in direct RF digitization. A dedicated GPS receiver is used in each receiver system to maintain the time alignment of the ADCs and to stabilize the data acquisition clock frequency. The GPS receiver is also used to trigger the data acquisition and to keep each computer clock synchronized.

4.2. Data Processing Algorithm

[20] In CAPRI, the first step of the processing algorithm is to transfer the stored binary data files from each receiver location to a host computer for signal post processing. In early versions of passive radars [*Sahr and Lind*, 1997], data transportation was identified as one of the bottlenecks. CAPRI has been developed with real-time operation in mind; however, slow Internet connection speeds in rural areas remain a bottleneck. At the proposed receiver locations, which is discussed in section 5, connection

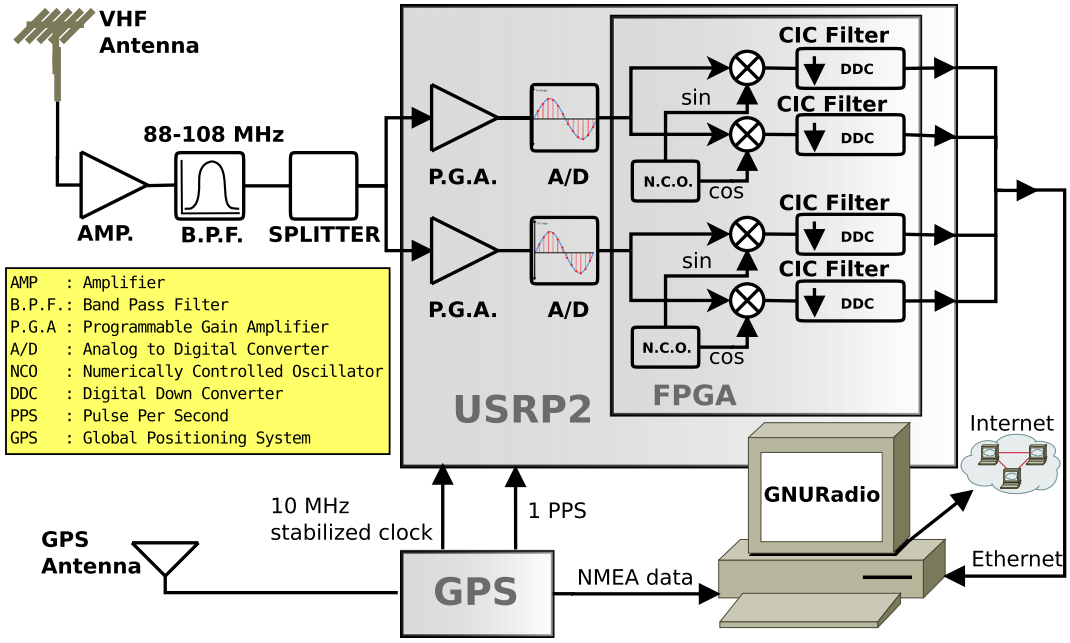

Figure 5. Block diagram of the CAPRI receiver.

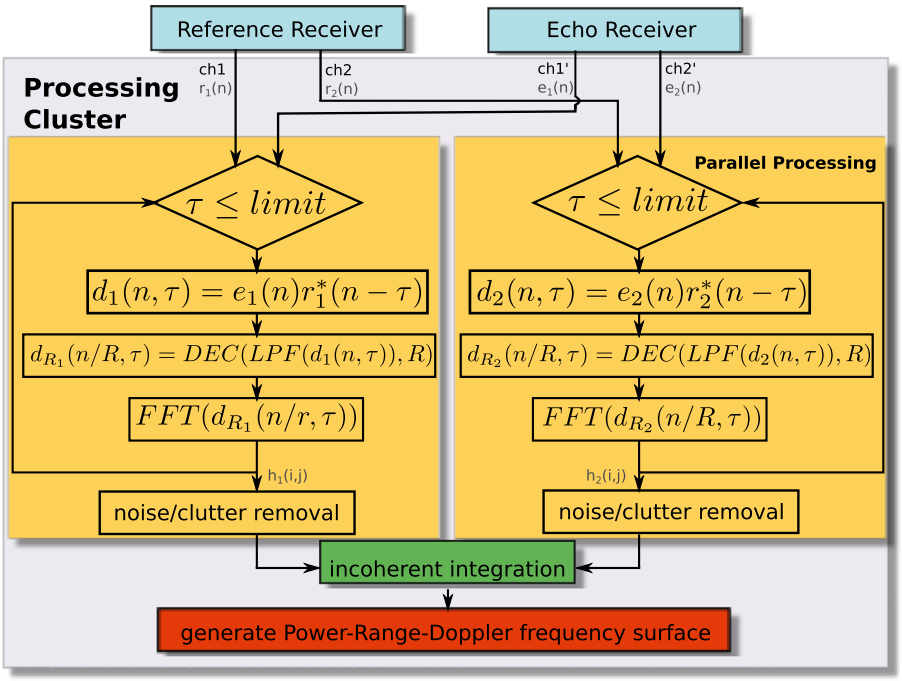

Figure 6. Block diagram of the data processing algorithm of CAPRI.

speeds obstruct the real-time processing capability. Hence, an adjustable duty cycle parameter is introduced in the acquisition algorithm to reduce the data rate. The continuous two-channel operation of CAPRI generates 140 Gb of data, by each receiver, for 1 day at 200 kHz bandwidth. This data amount can be reduced in half by introducing 50% duty cycle. The other parameter that can be used to reduce the data size is the signal bandwidth. Notice that most of the FM transmitter power is concentrated in the 90 kHz bandwidth. By decreasing the signal bandwidth to 100 kHz and operating at 50% duty cycle, in 1 day, CAPRI will produce 35 Gb of data which will be stored in each receiver.

[21] The second step in the signal processing algorithm is the computation of the Power-range-Doppler (PRD) frequency surfaces. This is achieved by calculating the two-dimensional discretized cross-correlation function:

$$|\chi[\tau,\upsilon]| = \left|\sum_{n=o}^{N-1} e[n]r^*[n-\tau]e^{-j2\pi\upsilon n/N}\right| \tag{4}$$

where

τ the delay,
υ the frequency difference of arrival (Doppler shift),
N the number of samples (integration time),
$e[n]$ and $r[n]$ the echo and reference signal vectors, respectively.

[22] We define the multiplication between the echo signal, $e[n]$, and the delayed complex conjugate of the received signal, $r^*[n-\tau]$, as detected signal, $d[n,\tau]$, throughout

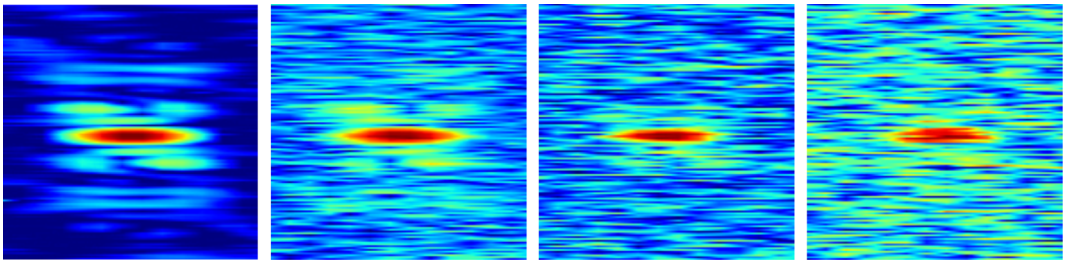

Figure 7. A simulated geophysical target is injected to the CAPRI FM data, and the SCR values are computed in differing noisy cases compared to the reference plot. (a) Reference PRD surface showing the simulated target. (b) Same simulated target in a noisy observation with SCR = 4.1244 dB. (c) Simulated target with the increased random noise on the observation SCR = 2.8821 dB. (d) Simulated target in excessive noise with SCR = 0.9030 dB.

Table 1. SCR and Peak-SCR Values of the Noisy PRD Surfaces and Incoherent Integration Results

Image	SCR (dB)	PSCR (dB)
Figure 7b	4.12444525306	19.9039202282
Figure 7c	2.88214249571	18.6616174709
Figure 7d	0.90303677264	16.6825117478
Figure 7b + Figure 7c	4.42772925908	20.2072042342
Figure 7b + Figure 7d	3.54541291523	19.3248878904
Figure 7c + Figure 7d	2.98861691943	18.7680918946

this section. A straightforward calculation of equation (4) requires the computation of the Fourier transform of $d[n, \tau]$ which makes the full baseband FM bandwidth available (e.g., $\pm$100 kHz for 200 kHz bandwidth). However, the expected Doppler frequency of the geophysical targets in which we are interested, such as equatorial electrojet, spread F, 150 km echoes, and meteors, are limited to 500 Hz at 100 MHz [*Hysell et al.*, 2007; *Hysell and Burcham*, 2002; *Chau et al.*, 2006]. Hence, the signal bandwidth can be reduced further by filtering and decimating the detected signal before applying the Fourier transform.

[23] In Figure 6, the outline of the CAPRI data processing algorithm is given. The implementation of this algorithm utilizes a cluster of computers which have four Intel Xeon E7 processors. This computational setup is required to carry out the data postprocessing in a parallel fashion in order to produce geophysical parameters in near real time. The algorithm presented in Figure 6 operates as follows; first, the channel pairs $r_1[n], e_1[n]$ and $r_2[n], e_2[n]$ from CAPRI receivers are combined to form the detected signals $d_1[n, \tau]$ and $d_2[n, \tau]$. Notice that the detected signals at different time delays are independent of each other and can be processed asynchronously in a parallel fashion. Second, $d_1[n, \tau]$ and $d_2[n, \tau]$ are filtered and decimated to capture the Doppler frequency bandwidth of interest while reducing the signal rate. In this process, finite impulse response (FIR) filters are used along with decimating polyphase filterbanks (DPFR), which are very powerful decimating filters for multirate signal processing tasks [*Harris et al.*, 2003]. Subsequently, applying the Fast Fourier Transform on $d_1[n, \tau]$ and $d_2[n, \tau]$ produces range-Doppler frequency matrices for channel 1, $ch1$, and channel 2, $ch2$. The cross-correlation process described here can be thought of as coherent integration. Thus, the integration gain, **G**, in the process can be given as the product of bandwidth, (**B**), and the correlation time in seconds, ($\mathbf{N/F_s}$), as $\mathbf{B} \times \mathbf{N/Fs}$. Accordingly, an integration (correlation) time of 0.1 s provide a processing gain of 40 dB for 100 kHz bandwidth which is found optimal for *E* region irregularities [*Sahr et al.*, 1997].

[24] The noise/clutter removal step uses a small section of the range-Doppler frequency matrices, where no targets are expected, to roughly estimate the numerical clutter floor which is then removed from each matrix element. Ultimately, incoherent integration of the resultant matrices is used to enhance the signal to clutter ratio (SCR) and produce the final PRD surfaces. The effect of the applied incoherent integration is evaluated in a simulated scenario. An imaginary target is injected in the CAPRI FM data, and in different noisy situations, PRD surfaces are produced. In Figure 7a, the original simulated target is shown. This figure is used as a reference to compute the SCR and Peak-SCR (PSCR) values of the noisy cases and are shown in Figures 7b, 7c, and 7d, with their incoherent integrations. The results are presented in Table 1.

[25] As expected, SCR values are improved with integration but if one of the PRD plots includes excessive noise, it slightly degrades the overall performance. Incoherent integration of multiple channels is not always optimal and can reduce or improve the overall PSCR value, which is directly related with the detectability. Thus, a preliminary self-ambiguity quality test on data is required. In CAPRI, detectability is greatly improved by the multichannel incoherent integration approach because it accumulates signal energy and smooths the noise (clutter) floor.

5. Location Study

[26] In Peru, there are more than 30 FM broadcasters (https://www.mtc.gob.pe/portal/comunicacion/concesion/radiodifusion/autorizadas_sonora.pdf) serving Lima that can be utilized for a possible passive radar setup. A list of FM broadcasters around Lima with transmitter powers above 20 kW is presented in Table 2. It can be inferred that the most powerful transmitters are located in Cerro

Table 2. FM Transmitters Serving Lima, Peru With Greater Than 20 kW of Effective Radiated Power

Station	Frequency	Power	Transmitter Location
F.M. S.O.S.S. 88.1 MHZ TELESTEREO 88 S.A.C.	88.1 MHz	20 kW	Cerro Marcavilca
MISORAS PERUANAS S.A.C.	89.7 MHz	25 kW	Cerro Marcavilca
PRODUCCIONES ASTURIAS S.A.C.	90.5 MHz	25 kW	Cerro Marcavilca
RADIODIFUSORA SAN BORJA S.R.L.	91.1 MHz	20 kW	Av. Javier Prado Este
RADIO TIGRE S.A.C.	91.9 MHz	20 kW	Cerro Marcavilca
STUDIO STEREO S.A.C.	92.5 MHz	25 kW	Cerro Marcavilca
CORPORACION RADIAL DEL PERU S.A.C.	93.1 MHz	20 kW	Cerro Marcavilca
RADIO "A" FRECUENCIA MODULADA S.A.C.	94.9 MHz	20 kW	Cerro Marcavilca
RADIO "Z" ROCK - POP S.A.C.	95.5 MHz	20 kW	Cerro Marcavilca
RADIO SAN LUIS S.A.C.	96.7 MHz	25 kW	Cerro Marcavilca
RADIO Y TELEVISION OMEGA S.A.	97.3 MHz	25 kW	Cerro Marcavilca
RADIO PANAMERICANA S.A.	101.1 MHz	25 kW	Cerro Marcavilca
RADIO UNION Y TV S.A.	103.3 MHz	20 kW	Cerro Marcavilca
EMPRESA RADIODIFUSORA EXCELSIOR S.A.C.	104.7 MHz	20 kW	Cerro Marcavilca
CORPORACION RADIAL DEL PERU S.A.C.	106.3 MHz	25 kW	Cerro Marcavilca
CORPORACION RADIAL DEL PERU S.A.C.	107.1 MHz	20 kW	Cerro Marcavilca
CORPORACION RADIAL DEL PERU S.A.C.	107.1 MHz	20 kW	Cerro Shangrilla
RADIO UNO S.A.C.	107.7 MHz	25 kW	Cerro Marcavilca

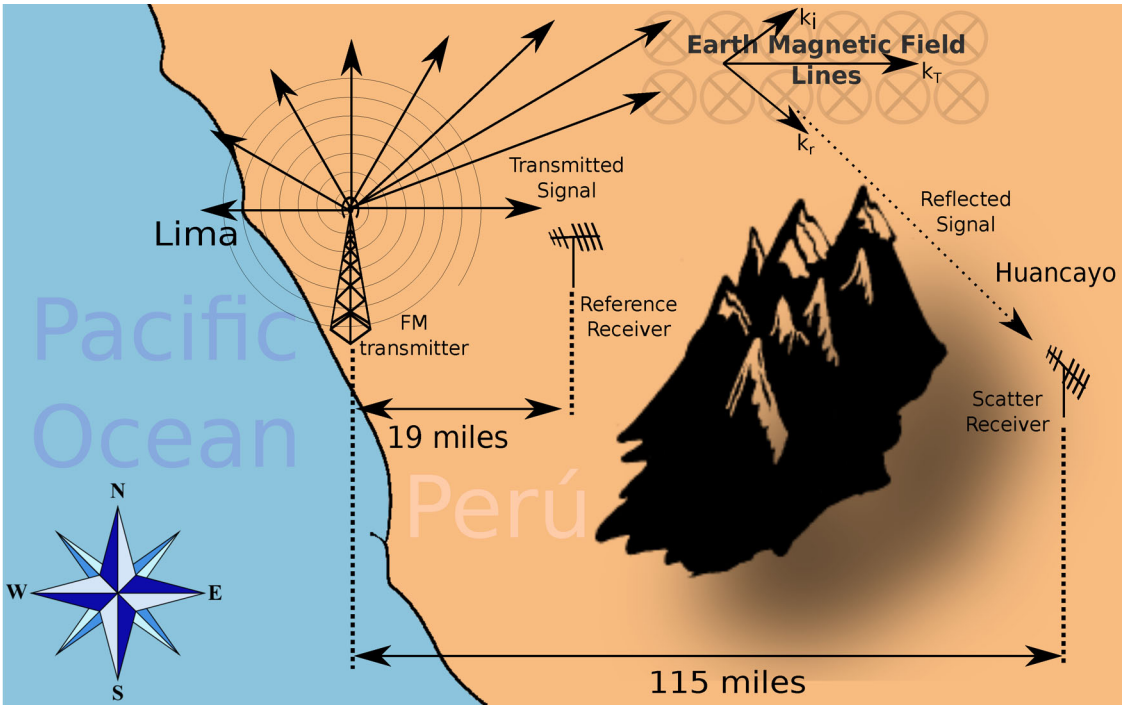

Figure 8. The geometry of the prospective dual receiver passive radar settlement in Peru, between Lima (latitude 11.9582°S, longitude 76.8589°W) and Huancayo (latitude 12.0379°S, longitude 75.3180°W).

Marcavilca (latitude 12.1841°S, longitude 77.0243°W), with up to 25 kW of peak power.

[27] A cluster of powerful FM transmitters that serve the same area has an excellent potential for a multichannel passive radar experiment. Also, the high mountains in Peru are convenient in blocking direct reception to the echo receiver. Besides these topological factors, infrastructure features such as sustained electricity, Internet connection, and housing for the receiver systems have to be taken into consideration for the receiver locations. An illustration of the proposed locations for a dual receiver, bistatic passive radar system is given in Figure 8. In the target area, the Andes mountains have North-to-South orientation, and they make excellent topographic shields for an East-to-West view. The proposed dual receiver design anticipates a reference receiver located at the Jicamarca Optical Observatory (latitude 11.9582°S, longitude 76.8589°W) near JRO to provide a nondistorted copy of the broadcasts from Lima, and an echo receiver located at the Huancayo Observatory (latitude 12.0379°S, longitude 75.3180°W).

[28] *F* region irregularities are strongly field-aligned [*Booker et al.*, 1938; *Goodwin et al.*, 1963; *Woodman*, 2009, and references therein]. These irregularities can only be detected when the radar **k**-vector is oriented perpendicular to

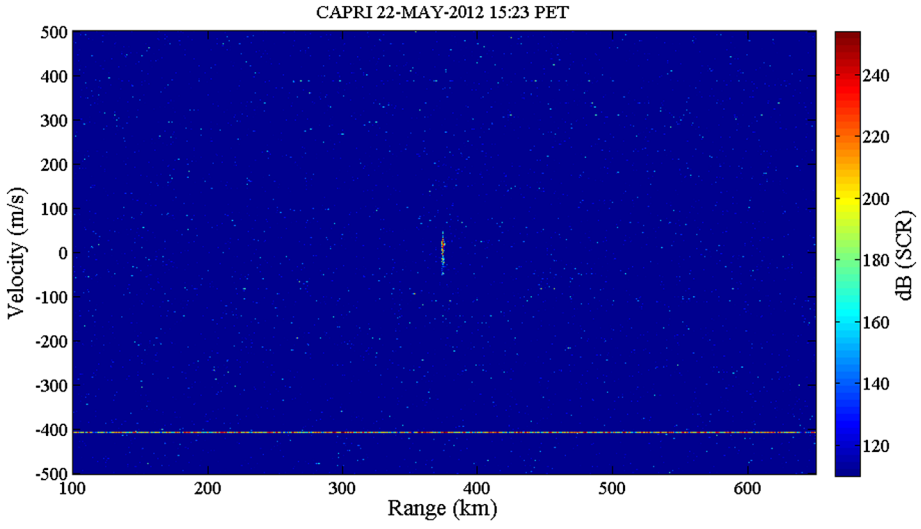

Figure 9. Range-velocity plot with a meteor trail echo from the CAPRI early testing data set of 22 May 2012 at 15:23 local time.

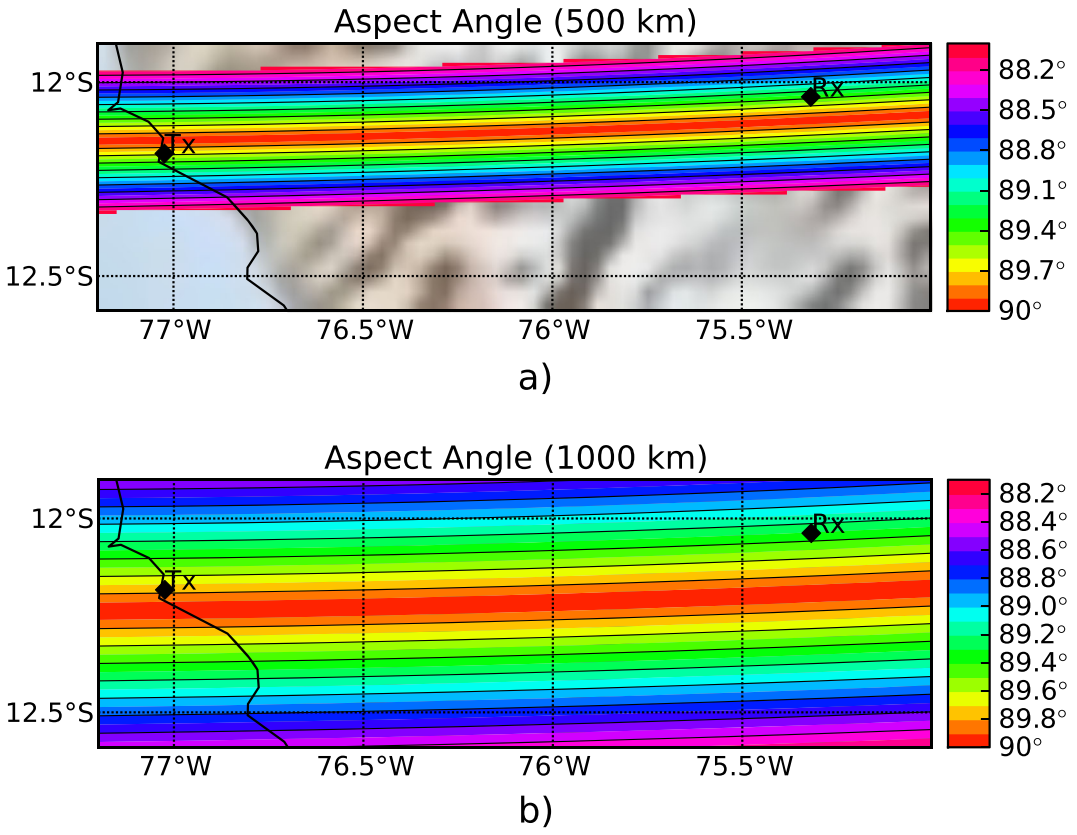

Figure 10. Bistatic aspect angle maps between the FM transmitters in Cerro Marcavilca, Lima and the echo receiver in Huancayo. (a) Aspect angle map in latitude versus longitude at 500 km height from the ground. Transmitter and receiver locations are marked in the map, and the perpendicular region is denoted as 90°. (b) Aspect angle map at 1200 km height.

the Earth's magnetic field lines [*Farley et al.*, 1996]. Thus, it is essential to analyze the aspect angles, where the bistatic radar **k**-vector is perpendicular to the Earth's magnetic field lines for the proposed radar system setup.

[29] Aspect angle maps between the transmitter location (Cerro Marcavilca) and the echo receiver location (Huancayo Observatory) are given in Figure 10. These plots were generated by using the 11th generation International Geomagnetic Reference Field (http://www.ngdc.noaa.gov/IAGA/vmod/igrf.html) (IGRF-11) model for year 2012. IGRF is a widely used mathematical model to compute the angle and the magnitude of the Earth's main magnetic field and its annular change rate at a given location. For a specific coordinate, the angle between the Earth's magnetic field and the radar **k**-vector from the transmitter to the receiver location ($\mathbf{k_i} + \mathbf{k_r} = \mathbf{k_T}$) gives the aspect angle at that position. We constructed Figures 10a and 10b by repeating this process at 500 and 1000 km altitudes, between latitudes 11.9°S–12.6°S and longitudes 75°W–77.2°W with incremental steps of 0.01° for each. The perpendicular region, where FAI scattering originates, is denoted as 90° in the figures, and it has a belt shape in the East-West direction. Notice that the orientation of this perpendicular region denotes parallel magnetic field lines in the South-North direction. Also, the perpendicular region gets wider with altitude while "drifting" to the south. This property of the magnetic field lines in the equatorial region was noticed in the past and used by JRO to make *F* region radar observations [*Woodman et al.*, 1976]. For the proposed receiver locations of CAPRI, the "drift" and the thickening in the perpendicular zone can be better seen in Figures 11a and 11b, where the altitude versus latitude change of the aspect angles are shown at longitudes 75.3180°W and 75.5000°W. The antenna beam of the echo receiver is pointed in the westward direction ensuring optimal reception of FAI scattering. In a previous study by Sahr [*Sahr et al.*, 2004], it was stated that using collinear-coaxial (COCO) antennas would be ideal when they are aligned with the magnetic north. Despite the COCO antennas being widely used with traditional radar systems, the narrow bandwidth is not suitable for a multichannel VHF passive radar operation. Our choice of wide-bandwidth log-periodic antennas are more suitable for a multifrequency SDR passive radar system.

[30] A meteor observation using a single log-periodic antenna from CAPRI is given in Figure 9. This event was captured during the testing phase of CAPRI in Peru (FM 89.7 MHz) at the proposed receiver locations on 22 May 2012 at 15:23 LT. Echoes appear at about 370 km range with a spectral peak of close to 80 m/s. Similar to the observations of Manastash Ridge Radar, there is a horizontal velocity line at around –400 m/s because of an interference on the receiver site [*Lind*, 1999].

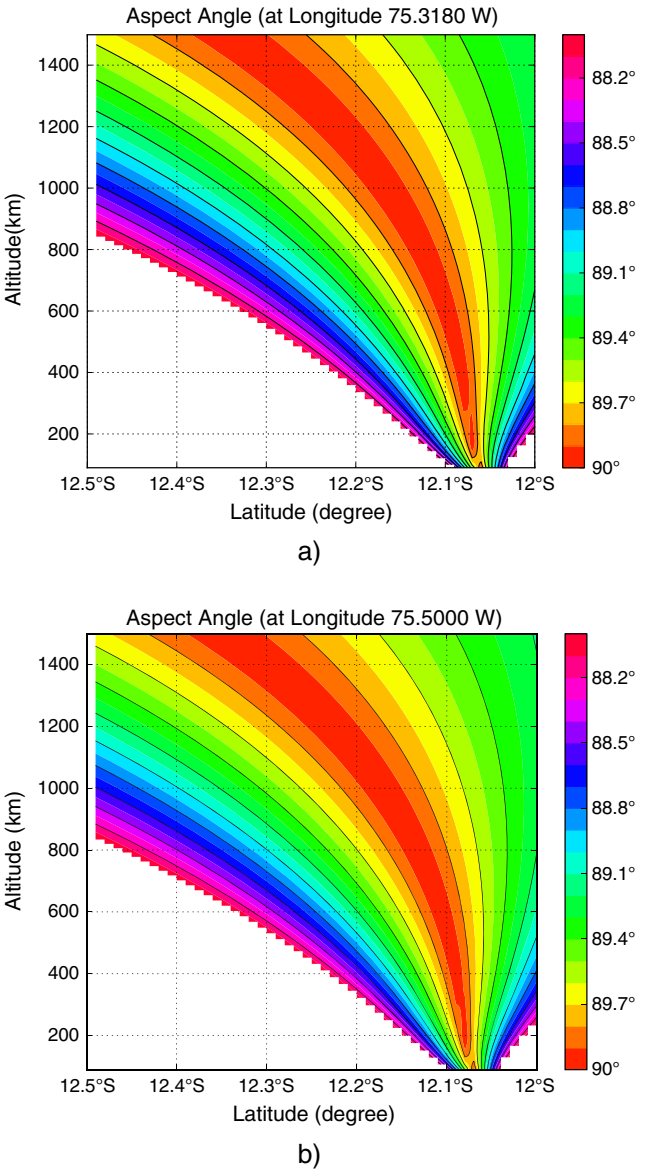

Figure 11. Bistatic altitude versus latitude aspect angle maps between the FM transmitters in Cerro Marcavilca, Lima and the echo receiver in Huancayo. (a) Change of the perpendicular region is shown at the echo receiver longitude (75.3180°W). (b) Altitude versus latitude aspect angle map at 75.5°W.

6. Concluding Remarks and Future Work

[31] In this paper, the development of a multifrequency passive radar setup for the equatorial ionospheric research named Coherent-scatter Atmospheric Passive Radar Imager (CAPRI) is described. In general, passive radar systems reduce the operational and maintenance costs, thus providing an economic alternative for long-term observations of the ionospheric irregularities. Furthermore, compared to the traditional hardware-based radar receivers, the digital receiver of the CAPRI and the SDR tools utilized in the data processing phase, provide a highly flexible, low-cost FM passive radar receiver that can also be easily modified for other frequency bands such as GSM and digital television broadcasts.

[32] Decisions on the deployment of passive radar systems are challenging. It involves considerations such as the geophysical properties of the region and the location of the transmitters and their effective radiated powers. Additionally, in the deployment process of CAPRI, detection of geomagnetic FAI scattering was the primary concern. Aspect angle maps for the CAPRI setup is presented to demonstrate the expected observation geometry for ionospheric *E* and *F* region observations.

[33] The next step is to deploy CAPRI near Lima, Peru, for continuous operation. Possible locations, Huancayo and Jicamarca Optical Observatory, are identified for the future operation. It is planned to make simultaneous observations at JRO with Jicamarca Unattended Long-term investigations of the Ionosphere and Atmosphere at other FM frequencies using the multichannel operation capability of CAPRI. It is also planned to increase the spatial coverage by including more receivers in the region.

[34] **Acknowledgments.** The authors would like to thank to John Mathews and James Breakall for their help and comments on the design process of the CAPRI. We also thank Z. Stephens, A. Hackett, F. Gallindo, and R. Sorbello for helping us in the preparation of this manuscript. This work is supported by the National Science Foundation under grants: AGS 1057038 and AGS 0457156 to Penn State University. The Jicamarca Radio Observatory is a facility of the Instituto Geofisico del Peru operated with support from the NSF AGS0905448 through Cornell University.

References

Baker, C., H. D. Griffiths, and I. Papoutsis (2005), Passive coherent location radar systems. Part 2: Waveform properties, *IEE Proc. Radar Sonar Navig.*, *152*, 160–168.

Booker, H. G., and H. W. Wells (1938), Scattering of radio waves by the F-region of the ionosphere, *J. Geophys. Res.*, *43*(3), 249–256.

Chau, J. L., and E. Kudeki (2006), Statistics of 150-km echoes over Jicamarca based on low-power VHF observations, *Ann. Geophys.*, *24*, 1305–1310.

Dillinger, M., K. Madani, and N. Alonistioti (2003), *Software Defined Radio: Architectures, Systems and Functions*, 1st ed., pp. 191–206, Wiley, Chichester, U. K.

Farley, D. T., and D. L. Hysell (1996), Radar measurements of very small aspect angles in the equatorial ionosphere, *J. Geophys. Res.*, *101*, 5177–5184.

Fejer, B. G., E. R. de Paula, R. A. Heelis, and W. B. Hanson (1995), Global equatorial ionospheric vertical plasma drifts measured by the AE-E satellite, *J. Geophys. Res.*, *100*(A4), 5769–5776.

Goodwin, G. L., and J. A. Thomas (1963), Field-aligned irregularities in the E_s-region, *J. Geophys. Res.*, *43*(3), 249–256.

Griffiths, H. D., and C. J. Baker (2005), Passive coherent location radar systems. Part 1: Performance prediction, *IEE Proc. Radar Sonar Navig.*, *152*, 153–159.

Griffiths, H. D., and N. R. W. Long (1986), Television-based bistatic radar, *J. Geophys. Res.*, *74*, 1205–1212.

Harris, F. J., C. Dick, and M. Rice (2003), Digital receivers and transmitters using polyphase filter banks for wireless communications, *IEEE Trans. Microw. Theory Tech.*, *51*(4), 1395–1412.

Hogenauer, E. (1981), An economical class of digital filters for decimation and interpolation, *IEEE Trans. Acoust. Speech Signal Process.*, *29*(2), 155–162.

Hysell, D. L., and J. D. Burcham (2002), Long term studies of equatorial spread *F* using the JULIA radar at Jicamarca, *J. Atmos. Sol. Terr. Phys.*, *64*(12–14), 1531–1543.

Hysell, D. L., J. Drexler, E. B. Shume, J. L. Chau, D. E. Scipion, M. Vlasov, R. Cuevas, and C. Heinselman (2007), Combined radar observations of equatorial electrojet irregularities at Jicamarca, *Ann. Geophys.*, *25*, 457–473.

Levanon, N. (1988), *Radar Principles*, 308 pp., Wiley-Interscience, New York.

Lind, F. (1999), Passive radar observations of the aurora, PhD thesis, University of Washington.

Martyn, D. F. (1955), Theory of height and ionization density changes at the maximum of a Chapman-like region, taking account of ion production, decay, diffusion and tidal drift, *Physics of the Ionosphere, Report of the Conference held at the Cavendish Laboratory, Cambridge, September, 1954. London: The Physical Society*, 254 pp.

Sahr, J., and F. Lind (1997), The Manastash Ridge radar: A passive bistatic radar for upper atmospheric radio science, *Radio Sci.*, *32*(6), 2345–2358.

Sahr, J., and M. Meyer (2004), Opportunities for passive VHF radar studies of plasma irregularities in the equatorial E and F regions, *J. Atmos. Sol. Terr. Phys.*, *66*(17), 1675–1681.

Siebert, W. M. (1956), A radar detection philosophy, *IRE Trans. Inf. Theory*, *2*(3), 204–221.

Stein, S. (1981), Algorithms for ambiguity function processing, *IEEE Trans. Acoust. Speech Signal Process.*, *29-3*, 588–599.

Tuysuz, B. (2012), Development and implementation of a passive VHF radar system using software defined radio techniques to study equatorial plasma instabilities near the Peruvian Andes, PhD thesis, Pennsylvania State University.

Woodman, R. F., and C. La Hoz (1976), Radar observations of F region equatorial irregularities, *J. Geophys. Res.*, *81*, 5447–5466.

Woodman, R. F. (2009), Spread F—An old equatorial aeronomy problem finally resolved?, *Ann. Geophys.*, *27*, 1915–1934.